Radboud Repository

Radboud University Nijmegen

PDF hosted at the Radboud Repository of the Radboud University Nijmegen

The following full text is an author's version which may differ from the publisher's version.

For additional information about this publication click this link.
http://hdl.handle.net/2066/32948

Rotational isomers of hydroxy deuterated o- and m-cresols studied by ultraviolet high resolution experiments

Grzegorz Myszkiewicz,[a] W.Leo Meerts,[a] Christian Ratzer,[b] and Michael Schmitt[b]

[a]*Molecular- and Biophysics Group, Institute for Molecules and Materials,*
Radboud University Nijmegen, P.O. Box 9010, NL-6500 GL Nijmegen, The Netherlands
[b]*Heinrich-Heine-Universität, Institut für Physikalische Chemie, 40225 Düsseldorf, Germany*
(Dated: April 27, 2005)

The laser induced fluorescence spectra of several torsional transitions of the $S_1 \leftarrow S_0$ electronic transition were recorded for the hydroxy deuterated o- and m-cresols. Both *cis* and *trans* rotamers were observed in a high resolution molecular beam experiment. The spectra were analyzed using a genetic algorithm assisted automatic assignment. The Hamiltonian used included rotational, torsional and rotation-torsion components. Both, high resolution rotationally resolved spectra and low resolution torsional frequencies, were combined to obtain the rotational constants, the direction of the methyl group axis, and the V_3 and V_6 barriers to internal rotation of the methyl top in the ground (S_0) and excited (S_1) states. The lifetime of the S_1 state is also reported. Quantum interference effects due to the interaction of the internal and overall rotation allowed for determination of the absolute sign of the angle between transition moment and the a principal axis.

I. INTRODUCTION

A large number of spectroscopic studies have been performed on substituted phenols. Of particular interest are substitutions in *ortho-* and *meta*-positions, because of the existence of *cis* − *trans* isomerism. Another important issue is the internal rotation of symmetric top groups attached to the benzene ring, like -CH_3. These two features meet in the o- and m-cresol molecules.

The *cis* and *trans* orientations of the hydroxy group were already predicted for some phenol derivatives in the thirties of the last century [1]. Similarly, in that decade the barrier to internal rotation of the methyl group was measured for the first time (for ethane) by Kemp and Pitzer [2]. Since then, phenol and toluene derivatives, among many other molecules, were shown to exhibit one or both of these characteristics.

The low resolution spectra of the o- and m-cresols were examined by many groups [3–7]. Both, *cis* and *trans* rotamers were identified and torsional parameters like the barrier to internal rotation (V_{3i} ($i = 1, 2$)) and the reduced rotational constant (F) of the methyl top were obtained for the ground (S_0) and excited electronic (S_1) states. Microwave spectra of o-cresols and their hydroxy deuterated isotopomers were recorded by Welzel *et al.* [8]. From these spectra accurate rotational and torsional parameters for the undeuterated and hydroxy deuterated o-cresols in the ground electronic state were determined.

The low resolution spectra revealed a drastic change of the barriers for the internal rotation upon electronic excitation from S_0 to S_1. This is consistent with the barriers derived for the other substituted toluenes, like fluorotoluenes [9, 10], toluidines [11] and tolunitriles [12]. For example, in *trans* o-cresol the internal rotation is strongly hindered ($V_3'' = 355$ cm^{-1}) in the ground state [4]. However, it decreases in the S_1 state by a factor of about four. On the other hand, the methyl rotor in *trans* m-cresol is almost free in S_0 ($V_3'' = 11$ cm^{-1}), but it is strongly hindered in S_1 ($V_3' = 213$ cm^{-1}) [3]. These changes could not simply be explained by steric effects. Several groups treated the problem theoretically [13–15]. Recently, Nakai and Kawai [16, 17] proposed the $\pi^* - \sigma^*$ hyperconjugation (HC) mechanism for ortho and meta substituted touluenes, which explains the aforementioned barrier changes upon the electronic excitation. Originally hyperconjugation was postulated to be the reason for conformational preferences in propene by Hehre *et al.* [13].

Rotationally resolved UV laser induced fluorescence (LIF) spectra provide accurate rotational constants for the ground and excited states of the examined molecules [18, 19], from which structural information can be deduced. Other important parameters like magnitude and direction of the transition moment (TM, to within its sign) and lifetime of the S_1 state can be determined [20]. Perturbations in the rotational spectra caused by internal rotation effects allow for more parameters to be derived [21]. Especially when combined with higher torsional transition frequencies they provide an accurate determination of the direction of the methyl top axis, the internal rotation constant, the barrier heights in the both electronic states and even the absolute direction of TM. The latter is obtained from quantum interference effects [21, 22]. In this paper we present frequency and intensity analysis of the high resolution, rotationally resolved LIF spectra of different torsional members of the $S_1 \leftarrow S_0$ transition in hydroxy deuterated o- and m-cresols.

The experimental spectra were analyzed with the help of Genetic Algorithm (GA) based automatic fitting procedures. These GA-fits are superior to classical assignments for very dense spectra and they allowed a fast and easy

assignment for the split spectra observed in this work.

II. THEORY

A. Model

All cresols studied are assumed to consist of the rigid planar frame (phenol) with a methyl group attached to it. The axis of the internal rotation of this methyl top a_{top} is in the plane of the benzene ring and makes an angle η with the a principal axis (see Figure 1). Since the electronic excitation takes place in the planar benzene chromophore we also assume the transition moment in the ab plane and with an angle θ with the a principal axis (Figure 1). The implemented model utilizes the principal axes of the molecule as a reference coordinate system (PAM method). The derived rotational constants do not include contributions from internal rotation and are directly related to the geometry of the molecule. Only the main features of the theory are presented below and more details can be found in [21, 23, 24].

The Hamiltonian, which describes the rotation-torsion problem consists of three parts: the rotational part H_r, the torsional part H_t and the coupling term between overall and internal rotation H_{rt}

$$H = H_r + H_t + H_{rt},\tag{2.1}$$

where

$$\begin{aligned}
H_r &= AJ_a^2 + BJ_b^2 + CJ_c^2 + F(\vec{\rho} \cdot \vec{J})^2, \\
H_t &= FJ_\alpha^2 + \frac{1}{2} \sum_{i=1,2} V_{3i}(1 - \cos 3i\alpha), \\
H_{rt} &= -2F\vec{\rho} \cdot \vec{J} J_\alpha.
\end{aligned}\tag{2.2}$$

where A, B, C are the rotational constants, J_g ($g = a, b, c$) are the projections of the total angular momentum $\vec{J}$ on the principal axes of inertia of the molecule and vector $\vec{\rho}$ has the following components

$$\rho_g = \frac{\cos \eta_g I_\alpha}{I_g}.\tag{2.3}$$

In the last equation I_α is the moment of inertia of the internal rotor and I_g are the principal moments of inertia of the whole molecule. For the cresol molecules $\eta_c = 0$, $\eta_a = \eta$, hence $\eta_b = 90 - \eta$. The reduced rotational constant for internal rotation F is defined as

$$F = \frac{\hbar^2}{2rI_\alpha} = \frac{F_\alpha}{1 - I_\alpha \sum_g \cos^2 \eta_g / I_g}.\tag{2.4}$$

J_α is the angular momentum of the internal rotor defined by $J_\alpha = -i\hbar \frac{\partial}{\partial \alpha}$ where α is the torsional angle and V_3 and V_6 are the three- and six-fold barrier heights of the periodic torsional potential.

A perturbation approach [18, 21, 23, 24] is used to derive the energy for (2.1). At first, the torsional Hamiltonian H_t is solved and the coupling between the internal and overall rotation H_{rt} is treated as the perturbation on the rotational Hamiltonian H_r. As a result one can construct an effective rotational Hamiltonian for every torsional state (labelled with $\nu\sigma$)

$$H_{\nu\sigma} = AJ_a^2 + BJ_b^2 + CJ_c^2 + F \sum_{n=1}^{\infty} W_{\nu\sigma}^{(n)} (\rho_a J_a + \rho_b J_b)^n,\tag{2.5}$$

where $W_{\nu\sigma}^{(n)}$ are the n-th order perturbation coefficients for the $\nu\sigma$ state. As shown in Ref. [23] these coefficients can be expressed as matrix elements of the internal rotation angular momentum operator J_α in the torsion-rotation basis. Here, ν labels the torsional level in the high barrier limit and σ takes the values $-1, 0, +1$. States with $\sigma = 0$ are nondegenerate of a symmetry and with $\sigma = \pm 1$ are two-fold degenerate of e symmetry. In the following we will label the levels with A and E.

In the calculations the Hamiltonian (2.5) is restricted to fourth order. In that case matrix elements (see Appendix B of Ref. [24]) connect rotational basis functions up to $\Delta K = 4$. A matrix of size $(2J + 1) \times (2J + 1)$ has to be diagonalized for every J for the νa and νe torsional states. The resulting eigenvalues are ordered with increasing energies and labelled with K_a and K_c as in a normal asymmetric rotor (for details see [25]).

B. Internal rotor effects

The transition frequencies follow the selection rules $\Delta J = 0, \pm 1$. Since the transition moment does not depend on the internal rotor angle additionally $\Delta \sigma = 0$ holds. We therefore expect for the $S_1 \leftarrow S_0$ origin two, more or less overlapping subbands, each with its own rotational structure. These subbands ($0a_1 \leftarrow 0a_1$ and $0e \leftarrow 0e$, A and E subbands, respectively) are separated by $\Delta \nu_0^{EA} = \Delta E'_{EA} - \Delta E''_{EA}$, where ΔE_{EA} are $E - A$ energy differences in the excited and ground states, respectively. If $\Delta \nu_0^{EA}$ is small both spectra partially overlap like in the o-cresols. A large value causes a complete separation of the subspectra as in the m-cresols. Furthermore, a decrease of the barrier upon electronic excitation results in a blue-shift of the E subband with respect to the A subband as observed in the o-cresols. For the m-cresols we observe a red-shift of the E subband and hence an increase of the torsional barrier upon electronic excitation.

The A- and E-subband pair have a different rotational structure. For the A states the odd perturbation coefficients vanish [23, 24] and it follows that this A subband has an asymmetric rigid rotor-like structure with effective rotational constants

$$
\begin{aligned}
A_A &= A + FW_A^{(2)} \rho_a^2, \\
B_A &= B + FW_A^{(2)} \rho_b^2, \\
C_A &= C + FW_A^{(2)} \rho_c^2.
\end{aligned} \tag{2.6}
$$

However, for the E states all the perturbation coefficients are nonzero giving rise to linear terms in K_a. This causes mixing of the rigid rotor wavefunctions, which induces transitions forbidden for a normal asymmetric rigid rotor [21].

For a transition moment in the ab plane (Figure 1) the line strengths are given by

$$
\begin{aligned}
A_{R''R'} &\propto |\mu_a \langle R'|\Phi_{Za}|R''\rangle|^2 + |\mu_b \langle R'|\Phi_{Zb}|R''\rangle|^2 + \\
&\quad + 2\mu_a \mu_b \langle R'|\Phi_{Za}|R''\rangle \langle R'|\Phi_{Zb}|R''\rangle,
\end{aligned} \tag{2.7}
$$

here the Z axis is the space-fixed axis determined by the laser polarization direction, $|R\rangle \equiv |J, K_a, K_c\rangle$, $\mu_a = \mu \cos\theta$, $\mu_b = \mu \sin\theta$, and μ is the absolute value of the TM. Φ_{Zg} are the direction cosines between the laboratory Z axis and the molecular g axis. Eq. (2.7) differs from the usual rigid rotor expression by an extra third term, the so-called interference term. As first pointed out by Plusquellic et $al.$ [22] and later by Remmers et $al.$ [21] the interference term can be used to determine the absolute sign of the θ angle. This is because $\mu_a \mu_b = 1/2\mu^2 \sin\theta \cos\theta$ and therefore changes sign with θ. The interference term is non-zero only for the E transitions. The final intensities are obtained by multiplying the line strengths with the temperature dependance. We used the two-temperature model defined in Ref. [26].

C. Computational approach

All the observed rotational spectra were fitted using GA based program. In general, the GA is a global optimizer, which uses concepts copied from the natural reproduction and selection processes. For a description of the GA the reader is referred to the original literature [27–29]. A more detailed description of the GA application to the fitting of high resolution spectra can be found in Ref. [30, 31]. Here, we only present the most important aspects of the GA fitting philosophy.

In the GA program each parameter from the model described in Sec. (II A) is represented by a gene. A vector of parameters (genes) that describe one spectrum is called a chromosome and a set of typically 300 chromosomes forms a population. Initially, all the parameters in the population are set randomly between limits imposed by a user. These limits depend on the degree of complication of the rotational spectra and can be as large as $\pm 10\%$ of the centrally chosen value. In practice, hardly any prior knowledge on the values of the parameters is required.

In the next step all the chromosomes from the population are evaluated by a fitness function F_{fg} (or cost function C_{fg}). This function is very critical for the GA to be successful. A more elaborate discussion on the choice of the cost function can be found elsewhere [30, 31]. The function used here is defined by Hageman et $al.$ [30] and can in the mathematical shorthand form be expressed as [31]

$$
C_{fg} = 100(1 - F_{fg}) = 100(1 - \frac{(f,g)}{||f||||g||}), \tag{2.8}
$$

where f and g represent the experimental and calculated spectra, respectively. The inner product (f,g) is defined with the metric W

$$
(f,g) = f^T W g \tag{2.9}
$$

and the norm of f defined as $\|f\| = \sqrt{(f,f)}$ (a similar definition holds for g). W has the matrix elements $W_{ij} = w(|j - i|) = w(r)$. For $w(r)$ we used a triangle function [30] with a user controlled width of the base Δw

$$w(r) = \begin{cases} 1 - |r| / \left(\frac{1}{2}\Delta w\right) & \text{for } |r| \leqslant \frac{1}{2}\Delta w \\ 0 & \text{otherwise.} \end{cases} \qquad (2.10)$$

After evaluation of the each chromosome from the population, the best solutions are kept for the next GA generation. This elitism prevents them from being lost and also chooses the best parents to be combined in the following crossover process. We use a two-point crossover, after which we apply a small number of mutations into just "born" chromosomes. Next the GA cycle (generation) repeats. For the cresol spectra we mostly set the maximum number of generations to 500.

The fitting approach to the experimental data was as follows. At first, we fit the A-subband of the $S_1 \leftarrow S_0$ origin to an effective asymmetric rigid rotor. Although this did not result in proper values for the rotational constants, it gave an indication which lines in the complicated rotational spectra belong to the A-subband. From the preliminary $0a_1 \leftarrow 0a_1$ subband fit the leftover E lines could be easily identified and the origin of the $0e \leftarrow 0e$ transition could be estimated. Hence this yielded an estimate of the torsional splitting $\Delta\nu_0^{EA}$. Combining these results and the knowledge of some torsional parameters from the literature a simultaneous GA fit of the $0a_1 \leftarrow 0a_1$ and $0e \leftarrow 0e$ subbands was quickly successful.

Line positions obtained from the GA fits were subsequently manually compared with the observed spectra and corrected if needed. Spectra of the higher torsional states ($1e \leftarrow 0e$ and $2a_1 \leftarrow 0a_1$ transitions) were also fit with the GA. Then, all the available data were fit by a separate least-squares based program [20]. Obtained parameters were utilized to improve the torsional origins and to refit all the data. After two or three such a steps a very good to perfect fit could be obtained with parameters that did not change any more within their uncertainties.

After the parameters that determine the line positions were found, we performed a simultaneous GA intensity fit of the $0a_1 \leftarrow 0a_1$ and $0e \leftarrow 0e$ subbands. All the parameters that did not affect the intensity were fixed. The lineshapes were fit using a Voigt profile with a fixed Gaussian contribution of 25 MHz (see Sec. (III)). Since the GA performs an intensity fit of the complete spectrum much better information on θ and the linewidth $\Delta_{Lorentz} \equiv \Delta_L$ is obtained than from an intensity fit to some selected individual lines. All errors presented in the paper are calculated from the combined available high and low resolution data.

We would like to note here that although the 'classical' assignment of quantum numbers to the experimental lines is still possible for the studied molecules it would be a very difficult, tedious and long process. If one considers one pair of spectra (A and E subbands) for one deuterated cresol, the 'classical' assignment of such a complicated spectra may easily take a month. Furthermore, assignment of the spectrum helps only for the fit of the higher torsional states of the same cresol molecule, but not for the other molecules. It is clear that only assignment of the rotationally resolved spectra of *cis* and *trans*, *o* and *m* cresols might have taken few months to half a year. In contrast the complete GA analysis of all the spectra presented in this publication took about one week. This is quite a gain of time, which can be spent on the actual analysis of the data, formulating hypothesis and making theoretical predictions.

D.   Ab initio calculations

The structure of *o*- and *m*-cresol in the electronic ground state has been optimized at the HF, MP2/6-31G(d,p) levels and at the CIS/6-31G(d,p) level for the electronically excited S_1-state with the Gaussian 98 program package (Revision11) [32]. The SCF convergence criterion used throughout the calculations was an energy change below 10^{-8} Hartree, while the convergence criterion for the gradient optimization of the molecular geometry was $\partial E/\partial r < 1.5 \cdot 10^{-5}$ Hartree/Bohr and $\partial E/\partial\varphi < 1.5 \cdot 10^{-5}$ Hartree/degrees, respectively.

III.   EXPERIMENTAL SETUP

The experimental setup for the rotationally resolved LIF is described elsewhere [33]. In short, the apparatus consists of a single frequency ring dye laser (Coherent 899-21), pumped with 6 W of the 514 nm line of an argon-ion laser. Rhodamine 110 is used in the dye laser as a lasing medium. The fundamental light from the dye laser is coupled into an external delta cavity (Spectra Physics) for second harmonic generation (SHG). The UV radiation at ~ 277 nm (for *m*-cresols) and at ~ 275 nm (for *o*-cresols) is generated in this cavity by an angle tuned, Brewster cut BBO crystal. The cavity length is locked to the dye laser frequency by a frequency modulation technique [34, 35].

The undeuterated cresols used in the experiment are commercially available substances. In order to substitute a hydrogen atom from cresols' -OH group with a deuterium atom, they are mixed with D_2O in the source container. To

increase the vapour pressure of cresols, the source is heated to 110° C. Subsequently, the molecular beam is formed by expanding a mixture from the source, seeded in 600 mbar of argon, through a 100 μm hole into the vacuum. The vacuum system is comprised of three differentially pumped vacuum chambers that are linearly connected by two skimmers (1 mm and 2 mm). The skimmers collimate the molecular beam and hence reduce the Doppler contribution to the measured linewidth. The UV laser crosses the molecular beam 360 mm downstream from the nozzle at right angles. The molecular fluorescence is collected perpendicular to the plane defined by the laser and molecular beam by an imaging optics that consists of a concave mirror and two plano-convex lenses. The Doppler contribution to the experimental linewidth in this set-up is 25 MHz of full width at half-maximum (FWHM). The total fluorescence is detected by a photomultiplier tube, whose output is digitized by a photon-counter and send to a PC for data acquisition and processing. The relative frequency is determined with a quasi-confocal Fabry-Perot interferometer with a free spectral range of 149.9434(56) MHz. For the absolute frequency calibration an iodine spectrum is recorded and compared with the available data [36].

IV. RESULTS

Four rotationally resolved torsional bands of the hydroxy deuterated *trans* o-cresol have been measured, *i.e.* $0a_1 \leftarrow 0a_1$, $0e \leftarrow 0e$, $1e \leftarrow 0e$ and $2a_1 \leftarrow 0a_1$. This allowed to determine not only the barriers to internal rotation, but also the torsional constant F in both electronic states. The ground state rotational constants and V_3'' were kept fix at the values of a microwave study [8], $\Delta \eta$ was fixed to zero and F_α'' was fixed to the value found for toluene [37]. Figure 2 shows the rovibronic spectrum of the split origin of *trans* o-cresol-d_1. The results of the fit to the rovibronic spectrum of the split origin and the frequencies of the $1e \leftarrow 0e$ and $2a_1 \leftarrow 0a_1$ are presented in Table I.

For the hydroxy deuterated *cis* o-cresol we detected only the $0a_1 \leftarrow 0a_1$ and $0e \leftarrow 0e$ torsional transitions. Like in undeuterated *cis* o-cresol this is due to the weak fluorescence signal from the higher torsional bands of the S_1 state [4]. Because of the limited number of torsional data we had to fix V_6 at zero in the both electronic states, F_α'' to a "typical" value for the -CH$_3$ rotor as found for toluene [37] and $\Delta F_\alpha = 0$ [43]. Furthermore, the ground state rotational constants and V_3'' were taken from a microwave study [8] and $\Delta \eta$ was fixed to zero. The final parameters from the simultaneous fit of the both subbands are given in Table II and a sample of the quality of this fit can be seen in Figure 3. This Figure illustrates the appearance of rovibronic transitions that are forbidden in an unperturbed rigid rotor spectrum from linear terms in K_a as described in section II B.

For the hydroxy deuterated *cis* and *trans* m-cresols we acquired similar torsional spectra as for the hydroxy deuterated *trans* o-cresol. However, the separation between $0a_1 \leftarrow 0a_1$ and $0e \leftarrow 0e$ origins in this case is very large (see Figure 4), resulting in no overlap of the rotational structure of both bands. We pasted together these spectra using iodine lines as a reference. This introduced an estimated error of 300 MHz in $\Delta \nu_0^{EA}$. In order to allow for the large error in $\Delta \nu_0^{EA}$ in the simultaneous fits of the $0a_1 \leftarrow 0a_1$ and $0e \leftarrow 0e$ bands we added an additional parameter $\Delta \widetilde{E}_{EA}$ with $\Delta \nu_0^{EA} = \Delta E'_{EA} - \Delta E''_{EA} + \Delta \widetilde{E}_{EA}$. This parameter helped in particular in the beginning of the fit procedure to relax constraints to the V_3 values, which are responsible for the A and E bands splitting and at the same time for the effects in the E band caused by the linear terms in the effective rotational Hamiltonian (Eq. 2.5). The final values of $\Delta \widetilde{E}_{EA}$ are on the order of few tens of MHz, which indicates that the estimated errors due to pasting two nonoverlapping spectra are at their upper limit. The final molecular constants for the hydroxy deuterated *trans* m-cresol are presented in Table III and a fit obtained with these parameters is compared with the experimental spectrum in Figure 4.

The parameters for the hydroxy deuterated *cis* m-cresol are given in Table IV and a sample of the fit is shown in Figure 5. This Figure compares the intensities of A- and E-lines for different relative signs of η and θ. Quantum interference effects are only observed for the E-lines. As Figure 5 shows, the fit with $\eta = -30.65°$, $\theta = -43.02°$ and $\eta = -30.65°$, $\theta = 43.02°$ for the A-lines is identical, while it differs considerably for the E-lines. Obviously, only the combination $\eta = -30.65°$ and $\theta = -43.02°$ gives the correct results. All torsional data for the hydroxy deuterated o- and m-cresols are summarized in Table V.

For all the aforementioned rotationally resolved spectra the GA intensity fit using the two-temperature model yielded typically values for the rotational temperatures $T_1 \sim 1.7$ K, $T_2 \sim 4$ K and for the weighting factor $w \sim 0.1$.

V. DISCUSSION

The methyl top barrier to internal rotation is very sensitive to the steric and electronic surrounding of the top. A more symmetric electron density around the carbon to which -CH$_3$ group is attached generally leads to lower barriers to internal rotation. Barriers to internal rotation for the undeuterated and hydroxy deuterated cresols obtained experimentally and theoretically by other groups [3, 4, 8, 17] are compared in Table VI. Not surprisingly, the current

values are similar to those from earlier experiments on the undeuterated cresols. Notable is the trend of a reduction of the barrier for hydroxy deuterated o-cresols and an increase of the barrier for m-cresols with electronic excitation.

The $S_1 \leftarrow S_0$ electronic transition in m- and o-cresol corresponds to a $\pi^* \leftarrow \pi$ transition. The CIS calculations show, that the first excited singlet state of $cis/trans$ m- and o-cresol is comprised mainly of two configurations: the first arises from a LUMO(χ_3) $\leftarrow$ HOMO(χ_2) excitation, the second arises from a LUMO+1(χ_4) $\leftarrow$ HOMO-1(χ_1) excitation. Both configurations contribute significantly to the S_1-state:

$$\Psi_e(S_1, cis, ortho) = 0.60328(\chi_2\chi_3) - 0.35717(\chi_1\chi_4)$$
$$\Psi_e(S_1, trans, ortho) = 0.61198(\chi_2\chi_3) - 0.33890(\chi_1\chi_4)$$
$$\Psi_e(S_1, cis, meta) = 0.61041(\chi_2\chi_3) - 0.34334(\chi_1\chi_4)$$
$$\Psi_e(S_1, trans, meta) = 0.60675(\chi_2\chi_3) - 0.35275(\chi_1\chi_4)$$

all with minor contributions from other configurations. Thus, a discussion of the changes of torsional barriers upon electronic excitation has to include at least the above molecular orbitals. We will start with a discussion of the barriers in m-cresol, since sterical reasons for the barrier are negligable here. Moreover, the meta positions do not communicate electronically with each other in contrast to the ortho and para positions. Figure 6 shows HOMO-1, HOMO, LUMO, and LUMO+1 of cis and $trans$ m-cresol for torsional angles of $0°$ (minimum of the potential) and $60°$ (maximum of the potential). The MO coefficients at the out-of-plane hydrogen atoms of the methyl group have been given numerically in the figure, for sake of clarity. The MO coefficients in the HOMO-1 and HOMO virtually do not change, as has been pointed out by Nakai and Kawai [16, 17]. Large changes can be seen in the LUMO and LUMO+1. For cis and $trans$ m-cresol the coefficients at the out-of-plane hydrogen atoms in the LUMO decrease upon rotation of the methyl group from the minimum conformation to the transitions state. The $\pi^* - \sigma^*$ hyperconjugation, which is responsible for this effect is denoted by the dotted lines in Figure 6. It can be described as a delocalization of the aromatic π^* electrons to the s-type hydrogen atom orbitals of the methyl group. Thus, hyperconjugation stabilizes the equilibrium conformation at $0°$, leading to a barrier increase upon electronic excitation, as observed in the experiment. The situation gets more complicated when including the LUMO+1 in the consideration. Here, the transition state conformation at $60°$ is stabilized, what in priciple should lead to a decrease of the barrier upon electronic excitation. The fact that both effects don't cancel out must be traced back to the different weights, that both configurations contribute to the S_1-state. The above coefficients for the linear combination of configurations show, that the LUMO contributes about three times as much as the LUMO+1. Furthermore, the coefficients show, that both configurations together contribute only to about 50 % of the excited state wave function.

The methyl torsional barrier of o-cresol, and especially that of cis o-cresol is much more influenced by steric interactions and/or intermolecular hydrogen bonds between the methyl and the hydroxy group than in m-cresol. While in m-cresol the minimum configuration is the same for the cis and $trans$ conformers, in cis o-cresol the minimum configuration changes between cis and $trans$. The in-plane hydrogen atom of the methyl group pointing towards the OH group describes the transition state for cis o-cresol and the minimum for $trans$ o-cresol (cf. Figure 7). This has been confirmed by normal mode analysis, which shows a negative frequency for the methyl rotation of the transition state structure of $trans$ o-cresol in Figure 7 and only positive frequencies for the minimum structure. The torsion represents the motion which mediates the transition over the top of the potential. The shift of the potential minimum by 60 ° might be explained by the possibility of an additional binding interaction between the in-plane hydrogen of the methyl group and the hydroxy group. For cis o-cresol the s-type MO coefficients of the methyl hydrogens in the LUMO increase upon rotation of the methyl group from the minimum to the transition state. This indicates a decrease of the barrier upon electronic excitation as observed in the experiment. On the other hand, the MO coefficients for the LUMO of $trans$ o-cresol decrease, implying a barrier increase upon electronic excitation, what can be traced back to the shift of the minimum by $60°$.

Tables VII and VIII show the calculated ground state rotational constants of cis and $trans$ o- and m-cresol, optimized at the MP2/6-31G(d,p) level of theory. The excited state rotational constants have been calculated with CIS/6-31G(d,p) and the change of the rotational constants upon electronic excitation as the difference of the CIS/6-31G(d,p) and the HF/6-31G(d,p) calculations. The calculated MP2 rotational constants are in very good agreement with the experimental ground state constants. The maximum deviations are 2%. Although the absolute rotational constants of the CIS calculations are in quite bad agreement with the excited state rotational constants, the difference between a HF calculation for the ground state and the CIS calculation for the excited state yields nearly perfect changes of the rotational constants upon electronic excitation. This is due to a cancellation of errors which arises from the neglect of dispersive interactions in both electronic states, but has a great predictive power for the estimation of the changes of rotational constants upon electronic excitation as has been shown to be valid for quite some different molecular systems [38, 39].

Using the program $pKrFit$ [40] we determined the structure of cis and $trans$ o- and m-cresol in the S_0 and S_1-states from the rotational constants, given in Tables I – IV. Due to the very limited number of inertial parameters, we

performed a fit limited to the r_0-structure, which neglects the vibrational contributions from the different isotopomers and which is based on the assumption:

$$I_0^g = I_{rigid}^g(r_0) \tag{5.11}$$

where the I_0^g are the (experimentally determined) zero-point averaged moments of inertia with respect to the inertial axes g. The functions $I_{rigid}^g(r_0)$ are calculated from the structural parameters r_0 using rigid-molecule formulas. Thus, no vibrational corrections are introduced in the determination of the structure. Table IX gives the results of the structure fits. As only three rotational constants are available we calculated the structure using a very simplified model for the molecules. In order to compare the structural changes upon electronic excitation, this model was chosen the same for all four isomers. All ring CH bonds are set to 108.5 pm for the electronic ground state and to 107.2 pm for the electronically excited state as in phenol. The methyl CH bonds are kept fix at 108.9 pm for both electronic states. The CC bond length of the ring-methyl group bond is kept at 150.6 pm. All dihedral angles are fixed at a planar conformation for both electronic states. The CC bonds between the hydroxy and methyl substituent are set equal and are fit (CC_b). All other ring CC bonds are set equal and are fit (CC_a). Additionally, the CO bond is fit. Of course the results of Table IX represent only one possible set of changes, that is valid in the given model.

The structural changes of *cis* and *trans* o- and m-cresol upon electronic excitation can be summarized by a shortening of the CO bond length and an overall increase of the ring CC bonds. These findings support the results of the *ab initio* calculations. Comparing the results of the CIS and the HF calculations, one finds a reduction of the CO bond length of 2 pm, independent of the conformer and an increase of the ring bond lengths between 1 and 4 pm.

As can be seen from our results, the torsional constant F_α slightly decreases upon electronic excitation ($\Delta F = -2.5\%$). This is consistent with a small weakening of the σ CH bonds in the methyl top and also supports the $\pi^* - \sigma^*$ HC mechanism [17]. The direction of the methyl top axis in all studied cresols almost bisects the CCC internal angle in the benzene ring (see Figure 1).

Due to the quantum interference effects we were able determine not only the magnitude, but also the absolute direction of the TDM (see Sec. (II B)). In all deuterated cresols θ has the same sign (direction) as η (see Figure 1). The transitions in the hydroxy deuterated *cis* cresols are of almost equal the a and b types, while in *trans* o-cresol the a type lines are stronger ($|\theta| = 37.00°$) and in *trans* m-cresol the b type character is more pronounced ($|\theta| = 50.95°$). Figure 8 shows the experimentally determined transition dipole moments for *cis* and *trans* ortho- and meta-cresol. The broken arrows indicate the direction of the TDM as obtained from the CIS/6-31G(d,p) calculations. In all four cases very close agreement between experiment and theory is obtained. If we compare the orientations of the TDM in the cresols with those of the parent molecules toluene and phenol (each in its own inertial system) we find, that the transition dipole moments of all four cresols are oriented close to that of phenol and almost perpendicular to that of toluene. This is quite different from the situation in m-aminophenol, studied by Reese *et al.*.[41] There, both substituents, the amino and the hydroxy group, contribute nearly equally to the resulting TDM. This was explained by a mixing of the zero-order states ^1L_a and ^1L_b through the unsymmetric substitution. The different behavior of the cresols can be explained by the absence of π-type molecular orbitals at the methyl group. Thus the "toluene" part of the molecule has no strong influence on the TDM orientation.

The fluorescence lifetime of the hydroxy deuterated cresols is similar to the S_1 state lifetime in hydroxy deuterated phenol ($\tau = 13.3(16)$ ns, Ref. [40]), except for the unusually long lifetime in hydroxy deuterated *trans* m-cresol ($\tau = 26.7(45)$ ns). The first suggests that like in phenol the rapid internal conversion to the -OH stretching vibration is blocked by a deuteration of the hydroxy group. The second is unexpected and it is somewhat similar to the long lifetime encountered in deuterated *cis* m-D, -OD phenol ($\tau = 38.8(70)$ ns, Ref. [40]).

VI. SUMMARY

We measured and analyzed the rotationally resolved torsional members of the $S_1 \leftarrow S_0$ electronic transition in hydroxy deuterated *o* and *m*-cresols. The spectra could be simulated by treating the internal rotation of the methyl top as a perturbation to the overall rotation of the molecules. For the analysis of the spectra we used the automated assignments based on genetic algorithms [30, 31], what facilitated the fitting of the complex spectra. The obtained barriers to internal rotation are similar to the ones reported for the undeuterated cresols and the changes in F_α and rotational constants upon electronic excitation seem to indirectly support the hyperconjugation $\pi^* - \sigma^*$ mechanism [17], which is held responsible for the large barrier changes upon the electronic excitation. The derived rotational constants in the both electronic states can be utilized for future validation of the geometry calculations of these molecules.

Other important parameters like the absolute direction of TM and the lifetimes of the hydroxy deuterated *o*- and *m*-cresols were determined. In all molecules the angle of the transition dipole moment with the inertial a-axis (θ) has the same sign (direction) as the angle of the methyl torsional axis with the inertial a-axis (η). This implies, that the

hydroxy group is the determining factor for the orientation of the TDM, while the influence of the methyl group is small.

The lifetime of these hydroxy deuterated cresols is similar to the lifetime previously reported for hydroxy deuterated phenol [40], with the exception of the hydroxy deuterated *trans m*-cresol, which has a factor two longer lifetime. Therefore explanations of the different lifetimes, which are based on conical intersections along a single (-OH) coordinate [42] have to be refined to account for the observations described in this study.

Acknowledgment

[1] Pauling, *J. Am. Chem. Soc.*, 1936, **58**, 94–98.

[2] J. Kemp and K. Pitzer, *J. Chem. Phys.*, 1936, **4**, 749.

[3] H. Mizuno, K. Okuyama, T. Ebata, and M. Ito, *J. Phys. Chem.*, 1987, **91**, 5589–5593.

[4] T. Aota, T. Ebata, and M. Ito, *J. Phys. Chem.*, 1989, **93**, 3519–3522.

[5] M. Schmitt *Laserspektroskopie wasserstoffbrückengebundener Cluster im Überschalldüsenstrahl.* PhD thesis, Ruprecht-Karls-Universität, Heidelberg, 1992.

[6] E. Fujimaki, A. Fujii, T. Ebata, and N. Mikami, *J. Chem. Phys.*, 2000, **112**, 137–148.

[7] K. Suzuki, Y. Emura, S. Ishiuchi, and M. Fujii, *J. Electron Spectrosc. Relat. Phenom.*, 2000, **108**, 13–20.

[8] A. Welzel, A. Hellweg, I. Merke, and W. Stahl, *J. Mol. Spec.*, 2002, **215**, 58–65.

[9] K. Okuyama, N. Mikami, and M. Ito, *J. Phys. Chem.*, 1985, **89**, 5617–5625.

[10] Z. Zhao, C. Parramenter, D. Moss, A. Bradley, E. Knight, and K. Owens, *J. Chem. Phys.*, 1992, **96**, 6362.

[11] K. Okuyama, N. Mikami, and M. Ito, *Laser Chem.*, 1987, **7**, 197–212.

[12] M. Fujii, M. Yamauchi, K. Takazawa, and M. Ito, *Spectrochim. Acta, Part A*, 1994, **50**, 1421–1433.

[13] W. J. Hehre, J. A. Pople, and A. J. P. Devaquet, *J. Am. Chem. Soc.*, 1976, **98**, 664–668.

[14] K. Lu, F. Weinhold, and J. Weisshaar, *J. Chem. Phys.*, 1995, **102**, 6787–6805.

[15] Y. Sonoda and S. Iwata, *Chem. Phys. Lett.*, 1995, **243**, 176–182.

[16] H. Nakai and M. Kawai, *Chem. Phys. Lett.*, 1999, **307**, 272–276.

[17] H. Nakai and M. Kawai, *J. Chem. Phys.*, 2000, **113**, 2168–2174.

[18] X. Q. Tan, W. A. Majewski, D. F. Plusquellic, and D. W. Pratt, *J. Chem. Phys.*, 1991, **94**, 7721–7733.

[19] G. Berden, W. L. Meerts, M. Schmitt, and K. Kleinermanns, *J Chem. Phys.*, 1996, **104**, 972–982.

[20] M. Schmitt, C. Ratzer, C. Jacoby, and W. Meerts, *J. Mol. Spectr.*, 2005.

[21] K. Remmers, E. Jalviste, I. Mistrik, G. Berden, and W. L. Meerts, *J. Chem. Phys.*, 1998, **108**, 8436–8445.

[22] D. F. Plusquellic and D. W. Pratt, *J. Chem. Phys.*, 1992, **97**, 8970–8976.

[23] E. Gordy and R. L. Cook, *Microwave Molecular Spectra*, John Wiley & Sons, New York, 3rd ed., 1984.

[24] D. R. Herschbach, *J. Chem. Phys.*, 1959, **31**, 91–108.

[25] J. T. Hougen, I. Kleiner, and M. Godefroid, *J. Mol. Spec.*, 1994, **163**, 559–586.

[26] Y. R. Wu and D. H. Levy, *J. Chem. Phys.*, 1989, **91**, 5278.

[27] J. H. Holland, *Adaption in Natural and Artificial Systems*, MI: The University of Michigan Press, Ann-Arbor, 1975.

[28] D. E. Goldberg, *Genetic Algorithms in search, optimisation and machine learning*, Addison-Wesley, Reading Massachusetts, 1989.

[29] I. Rechenberg, *Evolutionsstrategie - Optimierung technischer Systeme nach Prinzipien der biologischen Evolution*, Frommann-Holzboog, Stuttgart, 1973.

[30] J. A. Hageman, R. Wehrens, R. de Gelder, W. L. Meerts, and L. M. C. Buydens, *J. Chem. Phys.*, 2000, **113**, 7955–7962.

[31] W. L. Meerts, M. Schmitt, and G. Groenenboom, *Can. J. Chem.*, 2004, **82**, 804–819.

[32] M. J. Frisch, G. W. Trucks, H. B. Schlegel, G. E. Scuseria, M. A. Robb, J. R. Cheeseman, V. G. Zakrzewski, J. A. Montgomery, Jr., R. E. Stratmann, J. C. Burant, S. Dapprich, J. M. Millam, A. D. Daniels, K. N. Kudin, M. C. Strain, O. Farkas, J. Tomasi, V. Barone, M. Cossi, R. Cammi, B. Mennucci, C. Pomelli, C. Adamo, S. Clifford, J. Ochterski, G. A. Petersson, P. Y. Ayala, Q. Cui, K. Morokuma, P. Salvador, J. J. Dannenberg, D. K. Malick, A. D. Rabuck, K. Raghavachari, J. B. Foresman, J. Cioslowski, J. V. Ortiz, A. G. Baboul, B. B. Stefanov, G. Liu, A. Liashenko, P. Piskorz, I. Komaromi, R. Gomperts, R. L. Martin, D. J. Fox, T. Keith, M. A. Al-Laham, C. Y. Peng, A. Nanayakkara, M. Challacombe, P. M. W. Gill, B. Johnson, W. Chen, M. W. Wong, J. Andres, C. Gonzalez, M. Head-Gordon, E. S. Replogle, and J. A. Pople, Gaussian 98, revision a.11 Gaussian, Inc., Pittsburgh, PA, 2001.

[33] M. Schmitt, J. Küpper, D. Spangenberg, and A. Westphal, *Chem. Phys.*, 2000, **254**, 349.

[34] R.V. Pound, *Rev. Sci. Instrum.*, 1946, **17**, 490–505.

[35] R.W.P. Drewer and J.L. Hall and F.V. Kowalski and J. Hough and G.M. Ford and A.J. Munley and H. Ward, *Appl. Phys. B*, 1983, **31**, 97–105.

[36] S. Gerstenkorn and P. Luc, *Atlas du Spectre d'Absorption de la Molécule d'Iode*, CNRS, Paris.

[37] W. Kreiner, H. Rudolph, and B. Tan, *J. Mol. Spectr.*, 1973, **48**, 86–99.

[38] M. Schmitt, C. Ratzer, K. Kleinermanns, and W. L. Meerts, *Mol. Phys.*, 2004, **102**, 1605–1614.

[39] M. Schmitt, C. Ratzer, and W. L. Meerts, *J. Chem. Phys.*, 2004, **120**, 2752–2758.

[40] C. Ratzer, J. Küpper, D. Spangenberg, and M. Schmitt, *Chem. Phys.*, 2002, **283**, 153169.

[41] J. A. Reese, T. V. Nguyen, T. M. Korter, and D. W. Pratt, *J. Am. Chem. Soc.*, 2004, **126**, 11387–11392.

[42] A. L. Sobolewski and W. Domcke, *J. Phys. Chem.A*, 2001, **105**, 9275–9283.

[43] ΔP is defined as $P' - P''$, where P represents a particular parameter.

TABLE I: Deuterated (-OD) *trans* o-cresol molecular constants obtained from the combined fit of the rotationally resolved $0a_1 \leftarrow 0a_1$ and $0e \leftarrow 0e$ torsional transitions and origins of the torsional $1e \leftarrow 0e$ and $2a_1 \leftarrow 0a_1$ transitions.

	S_0		S_1	
A''	3 168.41479 [a]	ΔA	$-146.45(27)$	MHz
B''	2 173.76335 [a]	ΔB	$-5.69(23)$	MHz
C''	1 299.79054 [a]	ΔC	$-26.321(84)$	MHz
F_α	5.241053 [b]	ΔF_α	$-0.11491(62)$	cm^{-1}
V_3	371.047 [a]		83.415(14)	cm^{-1}
V_6	0 [c]		$-3.294(51)$	cm^{-1}
$\nu_0^{0a_1 \leftarrow 0a_1}$		36 201.093(10)		cm^{-1}
$\Delta\nu_0^{EA}$		40 019.7(68)		MHz
ΔE_{EA}	436.4(68)		40 456.1(68)	MHz
η	$-30.23(29)$	$\Delta\eta$	0 [c]	deg
θ		$-37.00(29)$		deg
τ		10.6(7)		ns

[a] Constants taken from microwave experiments [8] and fixed in the fit.
[b] Value for toluene [37].
[c] Fixed in the fit.

TABLE II: Deuterated (-OD) *cis* o-cresol molecular constants obtained from the fit of the rotationally resolved $0a_1 \leftarrow 0a_1$ and $0e \leftarrow 0e$ torsional transitions.

	S_0		S_1	
A''	3 232.91617 [a]	ΔA	$-104.61(22)$	MHz
B''	2 148.84054 [a]	ΔB	$-28.40(17)$	MHz
C''	1 301.65739 [a]	ΔC	$-26.710(62)$	MHz
F_α	5.241053 [b]	ΔF_α	0 [c]	cm^{-1}
V_3	669.10 [a]		88.8776(38)	cm^{-1}
$\nu_0^{0a_1 \leftarrow 0a_1}$		36 407.593(10)		cm^{-1}
$\Delta\nu_0^{EA}$		37 579.7(26)		MHz
ΔE_{EA}	15.4(26)		37 595.1(26)	MHz
η	$-31.76(12)$	$\Delta\eta$	0 [c]	deg
θ		$-45.65(12)$		deg
τ		14.9(14)		ns

[a] Constants taken from microwave experiments [8] and fixed in the fit.
[b] Value for toluene [37].
[c] Fixed in the fit.

TABLE III: Deuterated (-OD) *trans* *m*-cresol molecular constants obtained from the combined fit of the rotationally resolved $0a_1 \leftarrow 0a_1$ and $0e \leftarrow 0e$ torsional transitions and origins of the torsional $1e \leftarrow 0e$ and $2a_1 \leftarrow 0a_1$ transitions.

	S_0		S_1	
A''	3 653.36(56)	ΔA	$-114.66(30)$	MHz
B''	1 738.36(33)	ΔB	$-18.79(16)$	MHz
C''	1 186.90(20)	ΔC	$-20.570(73)$	MHz
F_α	5.286(12)	ΔF_α	$-0.130(32)$	cm^{-1}
V_3	3.188(180)		204.29(46)	cm^{-1}
V_6	0 [a]		$-28.42(30)$	cm^{-1}
$\nu_0^{0a_1 \leftarrow 0a_1}$		36 095.829(10)		cm^{-1}
ΔE_{EA}	161 089(300)		5 763(300)	MHz
$\Delta \widetilde{E}_{EA}$		11(300)		MHz
η	$-29.700(79)$	$\Delta \eta$	0 [a]	deg
θ		$-50.95(10)$		deg
τ		26.7(45)		ns

[a] Fixed in the fit.

TABLE IV: Deuterated (-OD) *cis* *m*-cresol molecular constants obtained from the combined fit of the rotationally resolved $0a_1 \leftarrow 0a_1$ and $0e \leftarrow 0e$ torsional transitions and origins of the torsional $1e \leftarrow 0e$ and $2a_1 \leftarrow 0a_1$ transitions.

	S_0		S_1	
A''	3 573.14(44)	ΔA	$-126.26(20)$	MHz
B''	1 761.84(24)	ΔB	$-9.97(12)$	MHz
C''	1 189.10(16)	ΔC	$-18.583(69)$	MHz
F_α	5.287(12)	ΔF_α	$-0.156(24)$	cm^{-1}
V_3	21.341(52)		221.82(32)	cm^{-1}
V_6	0 [a]		$-29.77(24)$	cm^{-1}
$\nu_0^{0a_1 \leftarrow 0a_1}$		35 980.896(10)		cm^{-1}
ΔE_{EA}	138 123(300)		4 325(300)	MHz
$\Delta \widetilde{E}_{EA}$		$-22(300)$		MHz
η	$-30.647(45)$	$\Delta \eta$	0 [a]	deg
θ		$-43.02(45)$		deg
τ		9.8(6)		ns

[a] Fixed in the fit.

TABLE V: Measured torsional frequencies of hydroxy deuterated *cis* and *trans*, *o*- and *m*-cresols used in the combined low and high resolution fits. All the frequencies are relative to the origins of the $0a_1 \leftarrow 0a_1$ transitions.

transition	*trans ortho*	*cis meta*	*trans meta*	
$0e \leftarrow 0e$	40.0183(68)	−133.820(300)	−155.326(300)	GHz
$1e \leftarrow 0e$	43.693(10)	72.242(10)	67.858(10)	cm^{-1}
$2a_1 \leftarrow 0a_1$	73.357(10)	142.698(10)	134.686(10)	cm^{-1}

TABLE VI: Comparison of the rotational barriers for the undeuterated and hydroxy deuterated (marked with [a]) *cis* and *trans*, *o*- and *m*-cresols. All values are given in cm^{-1}.

Ref.	*cis ortho*		*trans ortho*	
	V_3''	V_6''	V_3''	V_6''
exp. [4]	600	−30	355	−7
exp. [8]	661.4(38)		369.95(11)	
exp. [8][a]	669.10(50)		371.047(40)	
theor. [17]	629		366	
exp. *this work*[a]	669.10(50)		371.047(40)	
	V_3'	V_6'	V_3'	V_6'
exp. [4]	90	−5	83	−7
exp. [7]	90.2(3)	−22.1(7)		
theor. [17]	126		123	
exp. *this work*[a]	88.8776(38)		83.415(14)	
	cis meta		*trans meta*	
	V_3''	V_6''	V_3''	V_6''
exp. [3]	26	−9	11	−8
theor. [17]	37		12	
exp. *this work*[a]	21.341(52)		3.188(180)	
	V_3'	V_6'	V_3'	V_6'
exp. [3]	211	−39	213	−22
theor. [17]	268		241	
exp. *this work*[a]	221.82(32)	−29.77(24)	204.29(46)	−28.42(30)

TABLE VII: Rotational constants of cis and trans *o*-cresol from a MP2/6-31G(d,p) calculation for the electronic ground state. The difference of a CIS/6-31G(d,p) and a HF/6-31G(d,p) calculation are compared to the experimentally determined changes of the rotational constants upon excitation.

	MP2//6-31G(d,p)	CIS//6-31G(d,p)	CIS-HF//6-31G(d,p)	exp.	
		cis-o-cresol			
A''	3 242.2	-	-	3 232.91	[MHz]
B''	2 202.6	-	-	2 148.84	[MHz]
C''	1 322.4	-	-	1 301.66	[MHz]
A'	-	3 193.1	-	3 128.31	[MHz]
B'	-	2 203.7	-	2 120.44	[MHz]
C'	-	1 314.5	-	1 274.94	[MHz]
ΔA	-	-	-88.6	-104.61	[MHz]
ΔB	-	-	-26.6	-28.40	[MHz]
ΔC	-	-	-24.3	-26.71	[MHz]
		trans-o-cresol			
A''	3 293.0	-	-	3 168.41	[MHz]
B''	2 190.5	-	-	2 173.76	[MHz]
C''	1 326.1	-	-	1 299.79	[MHz]
A'	-	3 168.1	-	3 021.97	[MHz]
B'	-	2 223.7	-	2 168.07	[MHz]
C'	-	1 317.1	-	1 273.47	[MHz]
ΔA	-	-	-147.7	-146.45	[MHz]
ΔB	-	-	-0.2	-5.69	[MHz]
ΔC	-	-	-24.8	-26.32	[MHz]

TABLE VIII: Rotational constants of cis and trans *m*-cresol from a MP2/6-31G(d,p) calculation for the electronic ground state. The difference of a CIS/6-31G(d,p) and a HF/6-31G(d,p) calculation are compared to the experimentally determined changes of the rotational constants upon excitation.

	MP2//6-31G(d,p)	CIS//6-31G(d,p)	CIS-HF//6-31G(d,p)	exp.	
		cis-m-cresol			
A''	3 670.3	-	-	3 573.14	[MHz]
B''	1 789.5	-	-	1 761.84	[MHz]
C''	1 212.0	-	-	1 189.10	[MHz]
A'	-	3 613.5	-	3 446.88	[MHz]
B'	-	1 801.4	-	1 751.87	[MHz]
C'	-	1 211.0	-	1 170.52	[MHz]
ΔA	-	-	-110.8	-126.26	[MHz]
ΔB	-	-	-13.7	-9.97	[MHz]
ΔC	-	-	-18.5	-18.58	[MHz]
		trans-m-cresol			
A''	3 652.9	-	-	3 653.36	[MHz]
B''	1 797.0	-	-	1 738.36	[MHz]
C''	1 213.6	-	-	1 186.90	[MHz]
A'	-	3 599.9	-	3 538.70	[MHz]
B'	-	1 806.3	-	1 719.57	[MHz]
C'	-	1 211.7	-	1 166.33	[MHz]
ΔA	-	-	-111.7	-114.66	[MHz]
ΔB	-	-	-11.2	-18.79	[MHz]
ΔC	-	-	-17.6	-20.57	[MHz]

TABLE IX: Structural changes of *cis* and *trans* *o*- and *m*-cresol upon electronic excitation from a model structure, described in the text.

	S_0	S_1	Δ	
	cis-o-cresol			
CC_a	142.6	144.2	+1.6	[pm]
CC_b	139.7	144.2	+4.5	[pm]
CO	135.6	134.7	-0.9	[pm]
	trans-o-cresol			
CC_a	143.3	143.6	+0.3	[pm]
CC_b	137.6	145.1	+7.5	[pm]
CO	135.4	134.8	-0.6	[pm]
	cis-m-cresol			
CC_a	139.8	143.6	+3.8	[pm]
CC_b	140.3	141.4	+1.1	[pm]
CO	135.5	134.1	-1.4	[pm]
	trans-m-cresol			
CC_a	143.2	146.6	+3.4	[pm]
CC_b	138.2	140.0	+1.8	[pm]
CO	135.1	133.0	-2.1	[pm]

Figure 1   Structures of *trans* and *cis* rotamers of hydroxy deuterated *o*- and *m*-cresols. The principal axes are denoted by a, b, c, with c perpendicular to the benzene frame. Both angles, η and θ, are taken to be positive in the sense of rotation direction from a to b axis.

Figure 2   Experimental and fitted spectra of hydroxy deuterated *trans o*-cresol. (I) Full spectra. The zero in the frequency scale corresponds to the $0a_1 \leftarrow 0a_1$ origin at $36\ 201.093(10)$ cm^{-1}. The $0e \leftarrow 0e$ origin is located at $40.020(7)$ GHz. (II) a 10 GHz zoom-in to the part of the spectrum where both: $0e \leftarrow 0e$ and $0a_1 \leftarrow 0a_1$ spectra overlap.

Figure 3   Effects of the -CH$_3$ group internal rotation. Part of the R-branch of (I) the $0a_1 \leftarrow 0a_1$ and (II) the $0e \leftarrow 0e$ subbands of hydroxy deuterated *cis o*-cresol spectra. The anomalous lines (see text) are marked with their quantum numbers $(J''K_a''K_c'' \leftarrow J'K_a'K_c')$. Line with asterisk is not a single line. The frequency scale is relative to the $0a_1 \leftarrow 0a_1$ subband origin.

Figure 4   Experimental and fitted spectra of hydroxy deuterated *trans m*-cresol. (I) Full spectra with indicated $0e \leftarrow 0e$ and $0a_1 \leftarrow 0a_1$ subbands. The zero in the frequency scale corresponds to the $0a_1 \leftarrow 0a_1$ origin at $36\ 095.829(10)$ cm^{-1}. The $0e \leftarrow 0e$ origin is located at $-155.325(300)$ GHz. (II) a 5 GHz zoom-in of (a) the $0e \leftarrow 0e$ and (b) $0a_1 \leftarrow 0a_1$ spectra.

Figure 5   Example of the θ angle sign effect on hydroxy deuterated *cis m*-cresol spectra. As predicted from theory the sign of θ has no effect on the $0a_1 \leftarrow 0a_1$ subband intensities (I). In the $0e \leftarrow 0e$ part of the spectrum (II) only "Fit 1" predicts proper line intensities. The frequency scale is given relative to the $0a_1 \leftarrow 0a_1$ subband origin.

Figure 6   Molecular orbitals of *cis* and *trans* m-cresol for the minimum conformation ($\alpha = 0°$) and top of the barrier ($\alpha = 60°$). The $\pi^* - \sigma^*$ hyperconjugation is denoted by dotted lines.

Figure 7   Molecular orbitals of *cis* and *trans* o-cresol for the minimum conformation and top of the barrier. The $\pi^* - \sigma^*$ hyperconjugation is denoted by dotted lines.

Figure 8   Experimental (solid arrows) and calculated (broken arrows) transition dipole moment orientations in ortho- and meta-cresol. For details of the calculations see text.
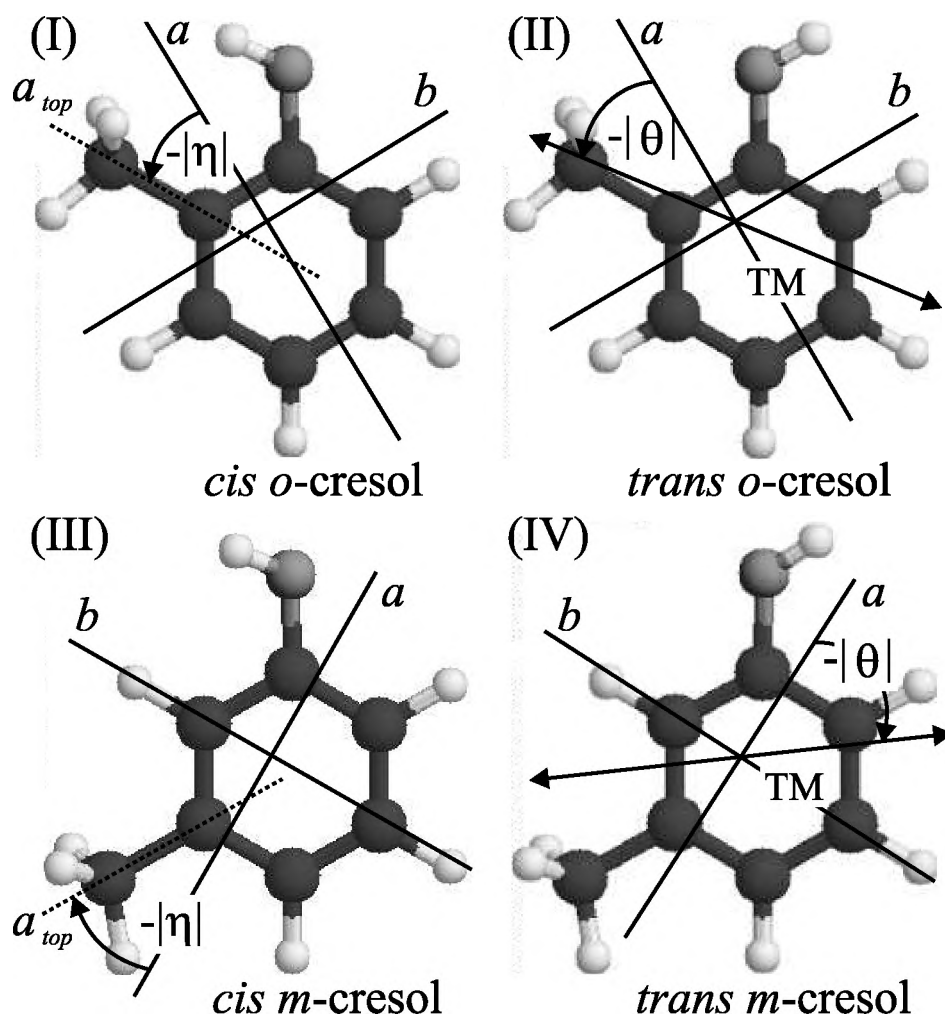
FIG. 1: Structures of *trans* and *cis* rotamers of hydroxy deuterated *o*- and *m*-cresols. The principal axes are denoted by a, b, c, with c perpendicular to the benzene frame. Both angles, η and θ, are taken to be positive in the sense of rotation direction from a to b axis.
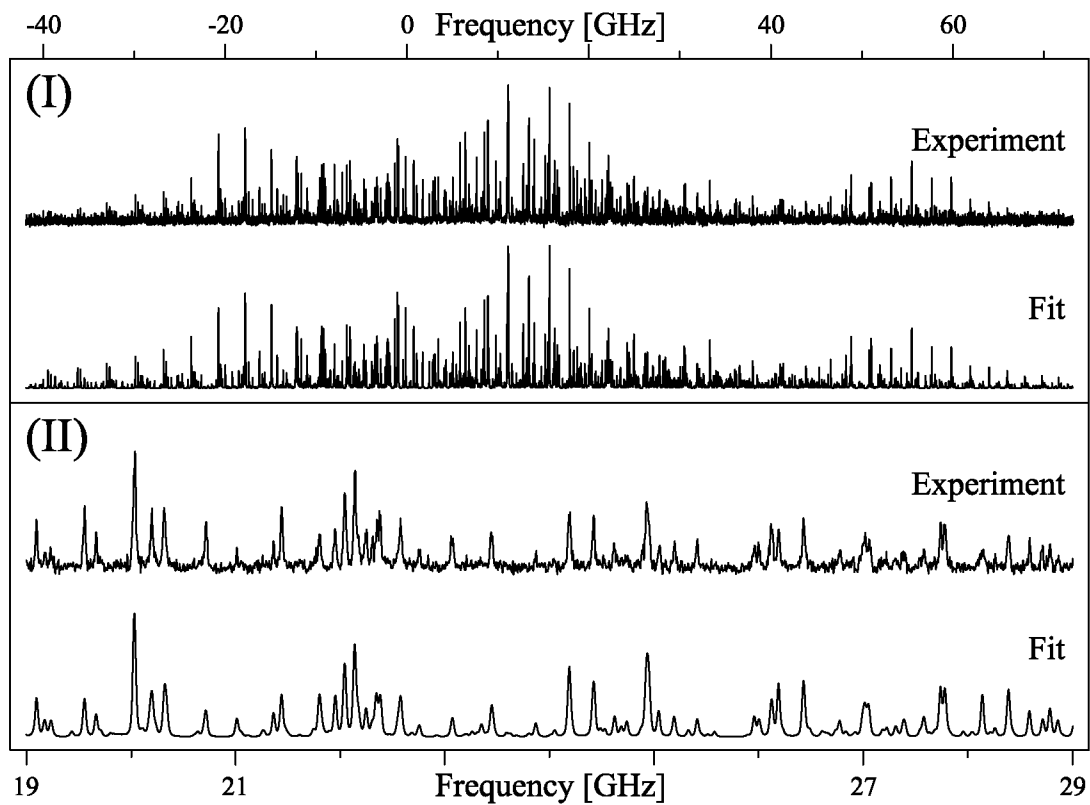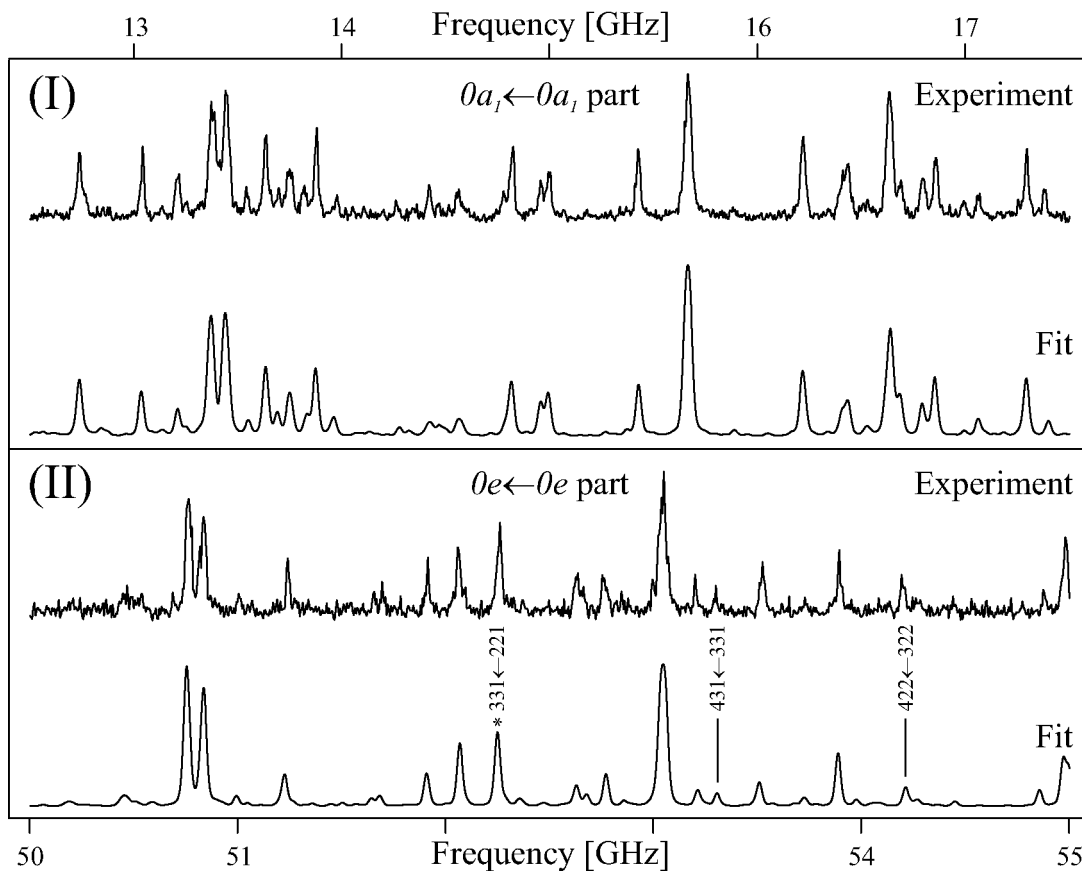
FIG. 2: Experimental and fitted spectra of hydroxy deuterated *trans* o-cresol. (I) Full spectra. The zero in the frequency scale corresponds to the $0a_1 \leftarrow 0a_1$ origin at 36 201.093(10) cm^{-1}. The $0e \leftarrow 0e$ origin is located at 40.020(7) GHz. (II) a 10 GHz zoom-in to the part of the spectrum where both: $0e \leftarrow 0e$ and $0a_1 \leftarrow 0a_1$ spectra overlap.

FIG. 3: Effects of the -CH$_3$ group internal rotation. Part of the R-branch of (I) the $0a_1 \leftarrow 0a_1$ and (II) the $0e \leftarrow 0e$ subbands of hydroxy deuterated *cis* o-cresol spectra. The anomalous lines (see text) are marked with their quantum numbers $(J'' K_a'' K_c'' \leftarrow J' K_a' K_c')$. Line with asterisk is not a single line. The frequency scale is relative to the $0a_1 \leftarrow 0a_1$ subband origin.
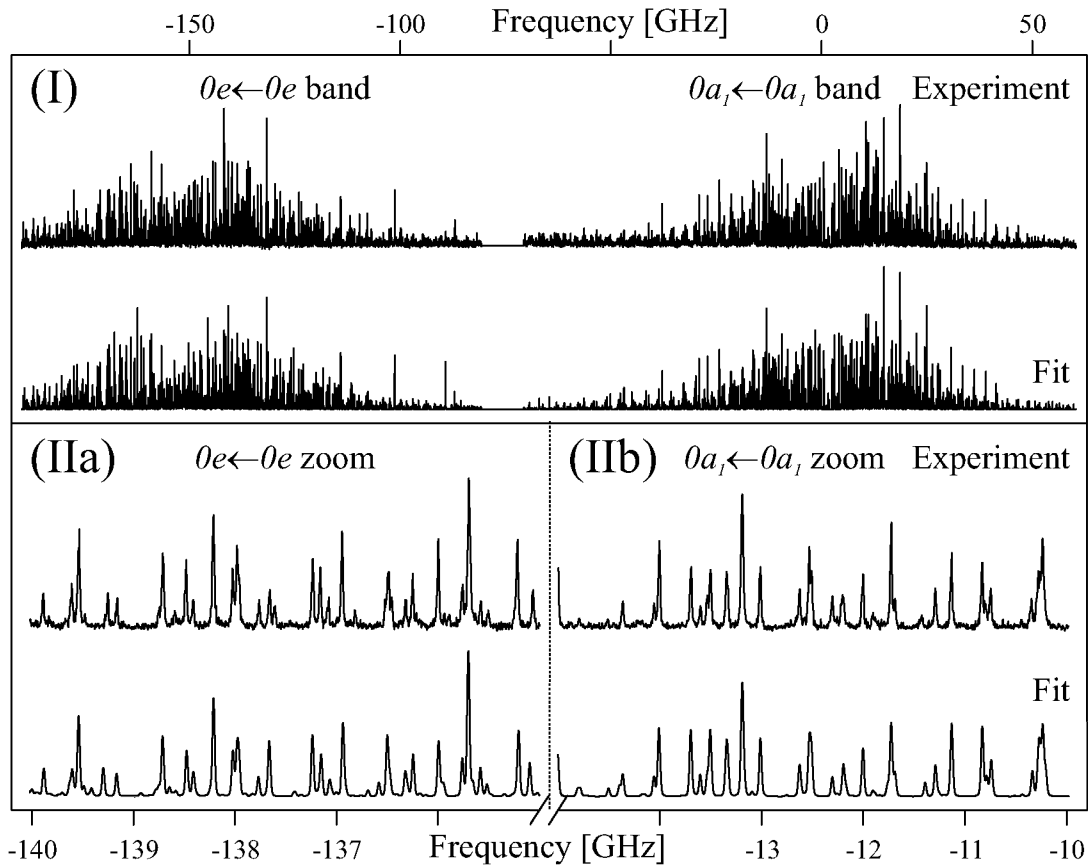
FIG. 4: Experimental and fitted spectra of hydroxy deuterated *trans* *m*-cresol. (I) Full spectra with indicated $0e \leftarrow 0e$ and $0a_1 \leftarrow 0a_1$ subbands. The zero in the frequency scale corresponds to the $0a_1 \leftarrow 0a_1$ origin at 36 095.829(10) cm^{-1}. The $0e \leftarrow 0e$ origin is located at $-155.325(300)$ GHz. (II) a 5 GHz zoom-in of (a) the $0e \leftarrow 0e$ and (b) $0a_1 \leftarrow 0a_1$ spectra.
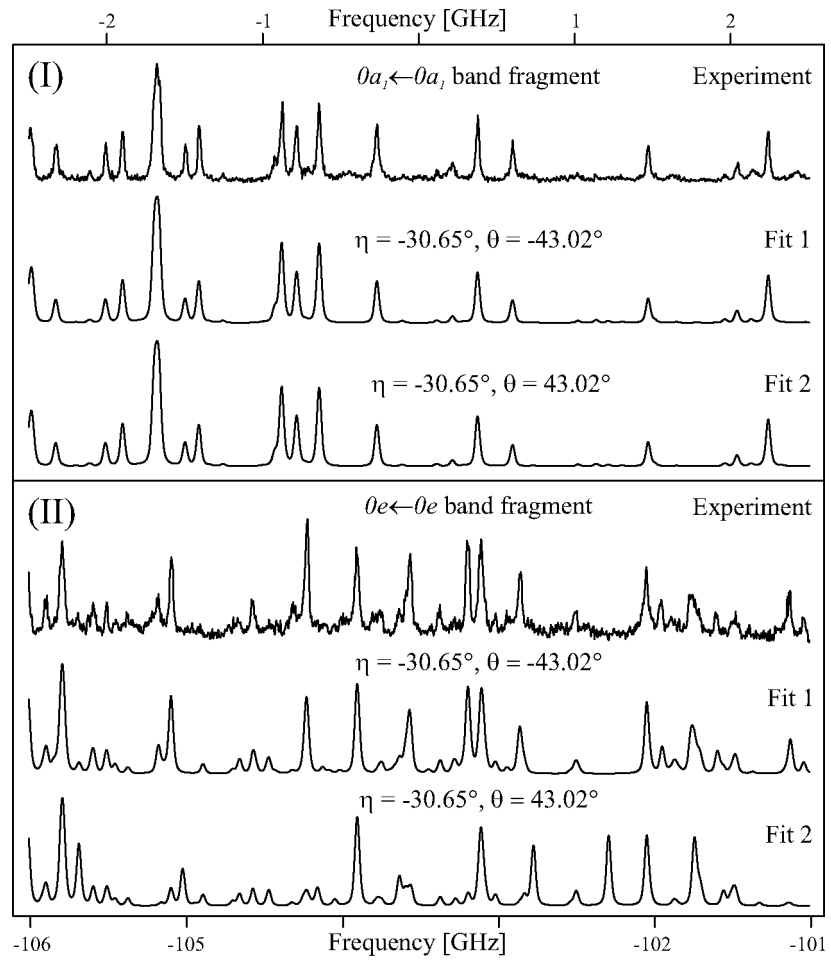
FIG. 5: Example of the θ angle sign effect on hydroxy deuterated *cis* m-cresol spectra. As predicted from theory the sign of θ has no effect on the $0a_1 \leftarrow 0a_1$ subband intensities (I). In the $0e \leftarrow 0e$ part of the spectrum (II) only "Fit 1" predicts proper line intensities. The frequency scale is given relative to the $0a_1 \leftarrow 0a_1$ subband origin.
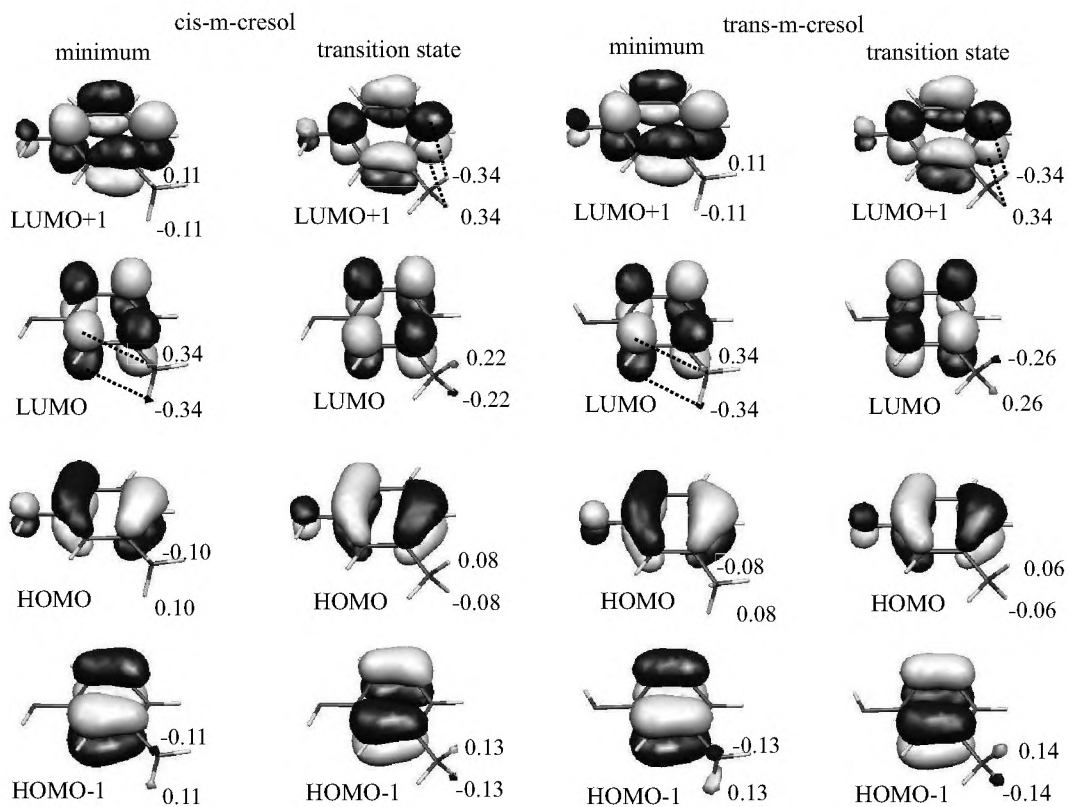
FIG. 6: Molecular orbitals of *cis* and *trans* m-cresol for the minimum conformation ($\alpha = 0°$) and top of the barrier ($\alpha = 60°$). The $\pi^* - \sigma^*$ hyperconjugation is denoted by dotted lines.
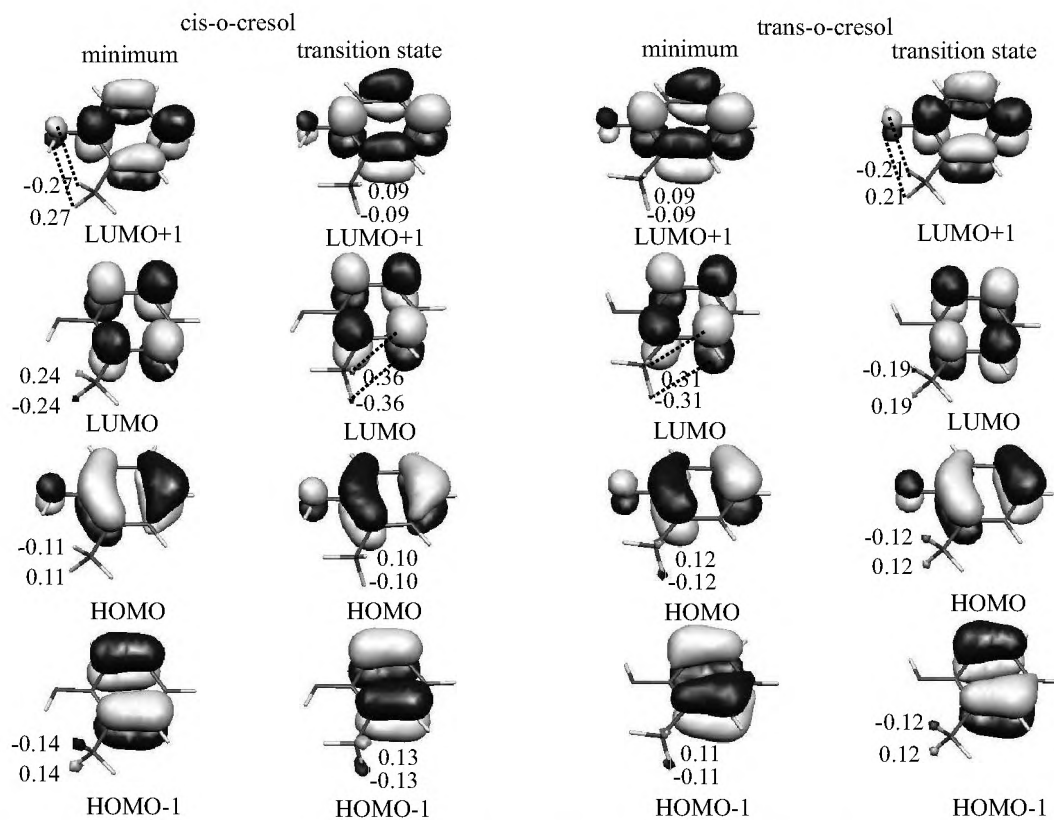
FIG. 7: Molecular orbitals of *cis* and *trans* o-cresol for the minimum conformation and top of the barrier. The $\pi^* - \sigma^*$ hyperconjugation is denoted by dotted lines.
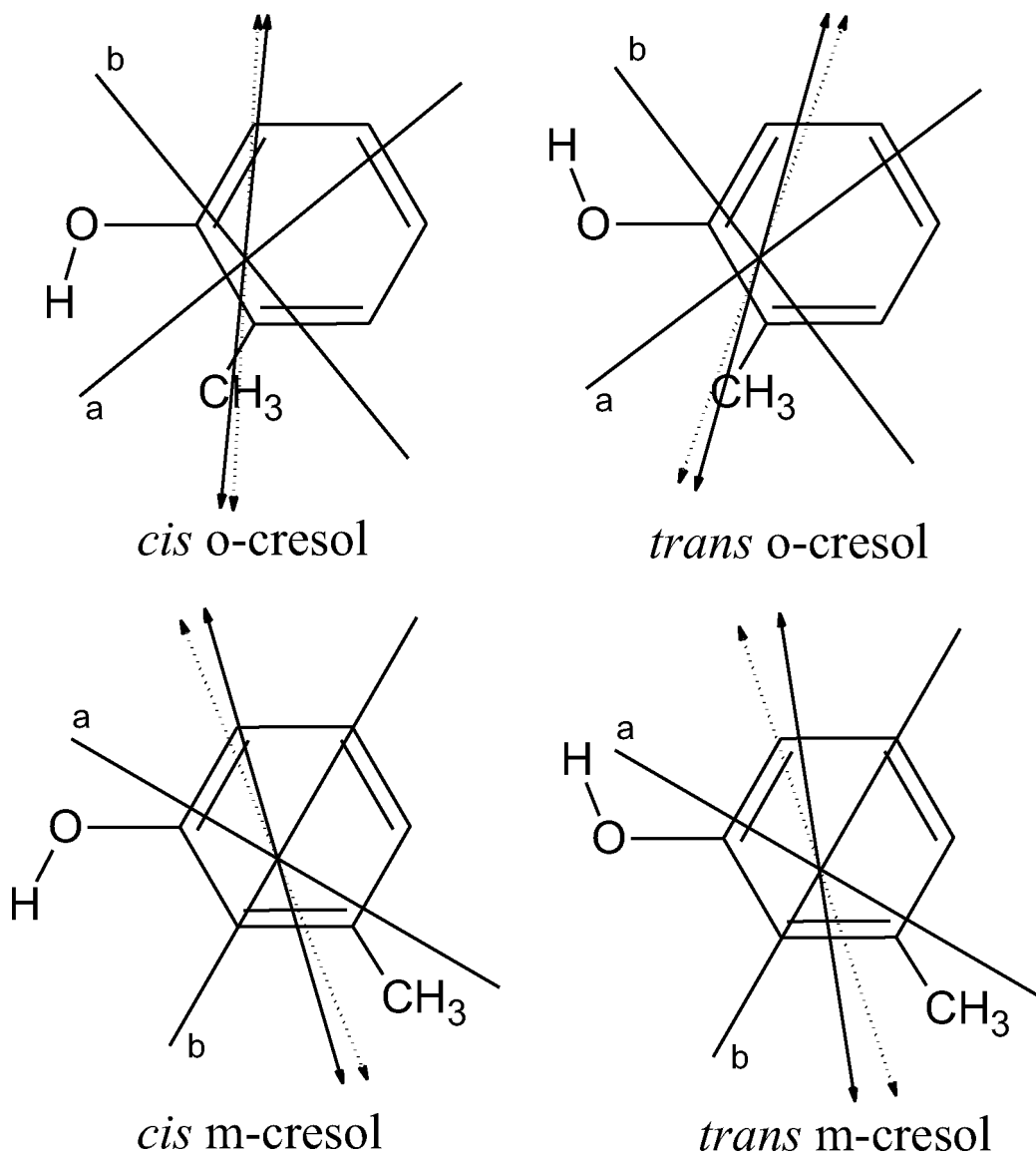
FIG. 8: Experimental (solid arrows) and calculated (broken arrows) transition dipole moment orientations in ortho- and meta-cresol. For details of the calculations see text.